J IRAN CHEM SOC
DOI 10.1007/s13738-017-1180-3

ORIGINAL PAPER

Structurally simple D–A-type organic sensitizers for dye-sensitized solar cells: effect of anchoring moieties on the cell performance

Praveen Naik[1] · Rui Su[2] · Dickson D. Babu[1] · Ahmed El-Shafei[2] · Airody Vasudeva Adhikari[1]

Received: 9 February 2017 / Accepted: 5 August 2017

Abstract In this work, we report synthesis and device fabrication studies of four metal-free D–A-type dyes (**A1**–**A4**) based on structurally simple *N,N*-dimethyl-4-vinyl aniline carrying four different acceptor/anchoring groups, as sensitizers for sensitizing photoanode (TiO_2). In the sensitizers, *N,N*-dimethylaniline ring acts as an electron donor, while barbituric acid, *N,N*-dimethyl barbituric acid, thiobarbituric acid and *N,N*-diethyl thiobarbituric acid function as electron acceptor/anchoring units. They were synthesized in good yield via Knoevenagel protocol in neutral condition without any catalyst. Further, they were subjected to structural, electrochemical and optical characterization in order to evaluate their structure, band gap and absorption/emission behavior. The studies reveal that all the four dyes have thermodynamic feasibility of electron injection as well as electron recombination; their optical band gaps were found to be in the range of 2.35–2.56 eV. High-quality crystals of **A2** and **A4** were grown by slow evaporation technique using its solution with 1:1 pet ether (60–80 °C)/ethyl acetate solvent mixture at room temperature. Their SC-XRD studies disclose that the crystals are in the triclinic system with space group *P*-1. Further, DFT studies were performed using Turbomole V7.1 software package to evaluate their optimized geometry and HOMO and LUMO levels. Finally, DSSC device fabricated with the dye **A1** showed relatively good efficiency when compared to other dyes mainly due to the effective binding of barbituric acid on the surface of TiO_2 through NH or OH functional group.

Electronic supplementary material The online version of this article (doi:10.1007/s13738-017-1180-3) contains supplementary material, which is available to authorized users.

✉ Ahmed El-Shafei
ahmed_el-shafei@ncsu.edu

✉ Airody Vasudeva Adhikari
avachem@gmail.com

[1] Organic Materials Laboratory, Department of Chemistry, National Institute of Technology Karnataka, Surathkal, Mangalore 575 025, India

[2] Polymer and Color Chemistry Program, North Carolina State University, Raleigh, NC 27695, USA

Published online: 20 August 2017

Graphical Abstract

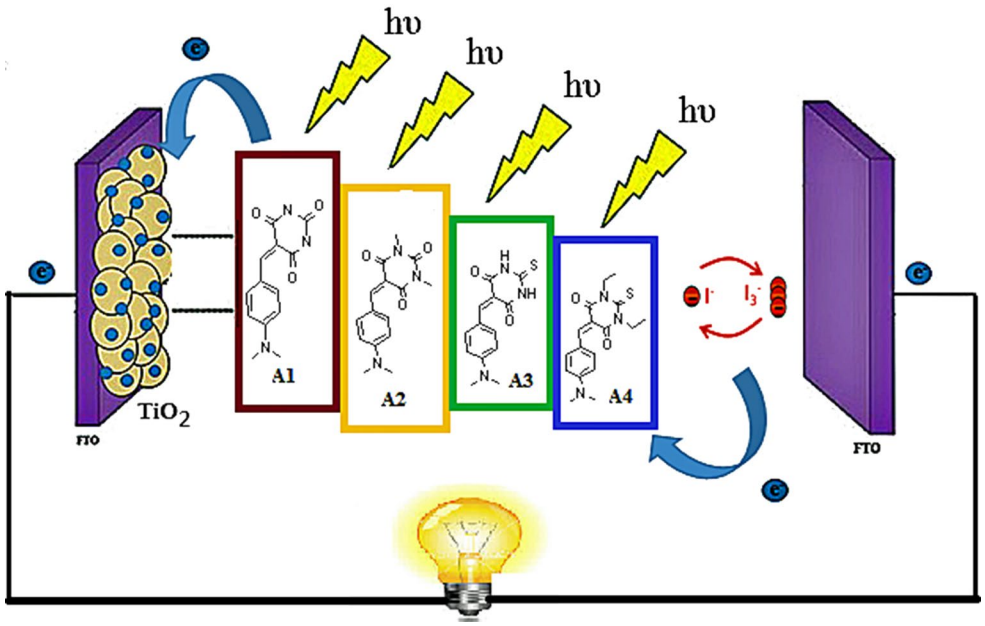

Keywords *n*-type sensitizer · DSSC · Barbituric acid · Knoevenagel condensation · DFT and TDFT calculations

Introduction

The quest for neat and cost-effective renewable energy has led to added research attention on organic photovoltaics. Over the past two decades, DSSCs have emerged as one of the best alternatives for silicon-based solar cells for harvesting solar energy after the report of pioneering work of Gratzel and coworkers in 1991 [1]. DSSC consists of mainly three components, viz. photoactive anode (usually TiO_2 semiconductor), a sensitizer, and an electrolyte, out of which the sensitizer plays a vital role in the photon conversion efficiency (η). Further, the sensitizers are broadly divided into two categories, i.e., metal-based complexes and metal-free organic dyes. The latter class of dyes possesses several advantageous over the metal-based sensitizers such as design versatility, high molar extinction coefficients, cost-effectiveness and relatively good efficiency. Therefore, a lot of efforts have been dedicated to the design and development of new metal-free organic dyes as potential sensitizers [2–4] for DSSC application.

A survey of the pertinent literature reveals that various design strategies such as D–A, D–π–A, D–A–π–A and D–D–π–A configurations are being used for developing new metal-free sensitizers with improved efficiency [3]. Among them, D–A-type architecture has attracted much attention mainly due to an efficient charge separation and easy movement of electron from donor to the acceptor moieties in the sensitizer. Moreover, such molecules exhibit an interesting optical property owing to intramolecular charge transfer (ICT) [5]. Normally, in D–A-type structures, the electron acceptor system acts as a good anchoring group, which binds chemically on the surface of the semiconductor TiO_2. Several organic chromophores, based on ammonia derivatives such as triphenylamine [6–11], diphenylamine [11], substituted anilines [12, 13], with "push–pull" structures have been reported as good sensitizers with decent photon conversion efficiency, when used in DSSCs. Obviously, *N,N*-dimethyl aniline [14, 15]-based dyes act as good donors because of their favorable electronic structure, i.e., the amino group attached to the phenyl ring plays an important role in the structural chemistry due to the ability of its lone pair of electron to interact with the π system of the benzene ring through *p*-π conjugation [16]. Further, the two methyl substituents on the nitrogen atom along with its lone pair enhance the electron density on the phenyl ring of substituted aniline. Also, its electron-donating capability is further enhanced due to its planar structure. In most of the aforesaid reports, cyanoacetic acid was used as an effective acceptor moiety along with substituted anilines as donors. Recently, many research groups have reported barbituric acid [17, 18] as an efficient acceptor/anchoring moiety when combined with a donor system because of its strong electron withdrawing nature and better anchoring capability on to the surface of semiconductor (TiO_2) through N–H or O–H functionality, which facilitates enhanced charge injection.

Against this background, in the present work, we synthesized four organic dyes derived from *N,N*-dimethyl-4-vinyl aniline with D–A-type configuration **(A1**–**A4)**, wherein *N,N*-dimethylaniline group functions as an electron donor, while barbituric acid, *N,N*-dimethyl barbituric acid, thiobarbituric acid and *N,N*-diethyl thiobarbituric acid act as electron acceptor/anchoring units. In the device, on photo-oxidation of these dyes, the electrons are expected to be delocalized from the planar 4-vinyl phenyl ring to electron-accepting barbituric acid conveniently. Then, the accumulated charge on electron acceptor moiety would be injected into the conduction band of TiO_2 through NH or OH binding [16]. This follows regeneration of the dye by I^-/I_3^- electrolyte system. Thus, it is anticipated that the synthesized dyes would show enhanced photon conversion efficiency in DSSCs.

The dyes were obtained from structurally simple and inexpensive 4-(*N,N*-dimethylamino)benzaldehyde in good yield following single-step Knoevenagel synthesis protocol (Scheme 1). The 3-D structures of **A2** and **A4** were confirmed by their SC-XRD studies. Furthermore, UV–visible absorption and photoluminescent emission studies were conducted in order to investigate their optical properties. Also, the dyes were subjected to cyclic voltammetry studies with the purpose of determining their electrochemical band gap as well as HOMO and LUMO levels. Density functional theory (DFT) and time-dependent density functional theory (TD-DFT) calculations with the def-TZVVP basis set were performed with the aim of acquiring knowledge on their optimized geometry and frontier molecular orbitals. Finally, **A1**–**A4** were applied as sensitizers toward the fabrication of DSSC to study their photovoltaic performance.

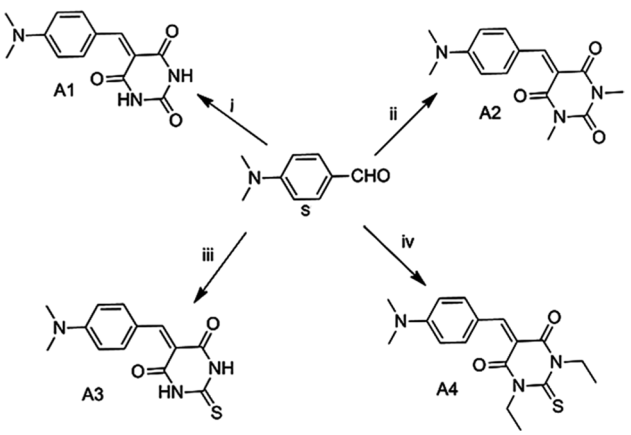

Scheme 1 Synthetic route of the chromophores **A1**–**A4**: (*i*) barbituric acid, ethanol, 60 °C, (*ii*) *N,N*-dimethyl barbituric acid, ethanol, 60 °C, (*iii*) thiobarbituric acid, ethanol, 60 °C, (*iv*) *N,N*-diethyl thiobarbituric acid, ethanol, 60 °C

Experimental

Materials and methods

The starting materials 4-(*N,N*-dimethylamino)benzaldehyde (**S**), barbituric acid, *N,N*-dimethyl barbituric acid, thiobarbituric acid and *N,N*-diethyl thiobarbituric acid were procured from Sigma-Aldrich and were used without purifying further. All the solvents were dried prior to use. The reaction progress was monitored by TLC technique. ^{1}H NMR and ^{13}C NMR spectra were recorded using a Bruker Avance 400 MHz using DMSO-d_6 as solvent and TMS as an internal standard. SC-XRD study was made using Bruker APEX duo II. UV–visible spectra of the dyes were recorded at room temperature using Analytik Jena Specord S 600 spectrophotometer, and FTIR spectra were run using Bruker Alpha spectrophotometer. The fluorescence spectra were recorded using Jasco FP6200 fluorescence spectrophotometer. The cyclic voltammetric (CV) measurements were taken on an Ivium Vertex electrochemical workstation in acetonitrile by using 0.1 M $(n\text{-Bu})_4N^+(BF_4)^-$ as supporting electrolyte. The CV experiments were conducted by using the three-electrode system, consisting of glassy carbon as the working electrode, platinum as a counter electrode and Ag/AgCl as a reference electrode, and data were recorded at a scan rate of 100 mV/s. Mass spectra were recorded on Thermo Scientific-EXACTIVE (ESI–MS), whereas the elemental analysis was carried out on a Flash EA1112 CHNSO analyzer (Thermo Electron Corporation). The DFT calculations were performed using Turbomole, V7.1 software package.

General method for synthesis of A1–A4

The dyes were synthesized as per the procedures reported [19–24] with small modifications. In the method, 4-(*N,N*-dimethylamino)benzaldehyde (**S**, 0.5 g, 3.355 mmol) was dissolved in 15 mL of absolute ethanol and to this respective barbituric acid derivative (4 mmol) dissolved in 10 mL of absolute ethanol was added slowly with stirring. The reaction mixture was further stirred at 60 °C for 10 h. The precipitated solid was filtered and washed with absolute ethanol. The dyes **A1**–**A4** were crystallized from appropriate solvents. Their characterization data are as follows:

5-(4-*N,N*-Dimethylaminobenzylidene)pyrimidine-2,4,6(1H,3H,5H)-trione (A1) Orange-colored solid crystallized from ethanol, yield 91%. ^{1}H NMR (400 MHz DMSO-d_6, ppm): 11.07 (s, 1H), 10.94 (s, 1H) 8.44–8.22 (d, J = 8 Hz, 2H), 8.16 (s, 1H), 6.81–6.79 (d, J = 8 Hz, 2H), 3.13 (s, 6H). ^{13}C NMR (400 MHz DMSO-d_6, ppm): 165.16, 163.19, 155.93, 154.63, 150.77, 139.52, 120.45, 111.67, 110.03. FTIR (ATR, cm^{-1}): 3442 (N–H stretching), 2945 (C–H stretching), 1678 (C=O stretching). TOF

HRMS ES + Calculated for $C_{13}H_{13}N_3O_3$: 259.2523. Found: 260.1164 $[M + H]^+$.

5-(4-*N,N*-Dimethylaminobenzylidene)-1,3-dimethyl-pyrimidine-2,4,6-trione (A2) Orange solid crystallized from dichloromethane, yield 90%. ^{1}H NMR (400 MHz DMSO-d_6, ppm): 8.44–8.42 (d, J = 7.2 Hz, 2H), 8.24 (s, 1H), 6.83–6.81 (d, J = 8 Hz, 2H), 3.23 (s, 6H). 3.14 (s, 6H), ^{13}C NMR (400 MHz DMSO-d_6, ppm): 163.72, 161.66, 156.80, 154.73, 151.73, 139.58, 120.49, 111.68, 109.79, 28.98, 28.36, FTIR (ATR, cm^{-1}): 3040.70 (C–H stretching), 1652 (C=O stretching). TOF HRMS ES + Calculated for $C_{15}H_{17}N_3O_3$: 287.3041. Found: 288.1443 $[M + H]^+$.

5-(4-*N,N*-Dimethylaminobenzylidene)-2-thioxo-dihydro-pyrimidine-4,6(1H,5H)-dione (A3) Red solid crystallized from ethanol, yield 85%. ^{1}H NMR (400 MHz DMSO-d_6, ppm): 12.16 (s, 1H), 12.06 (s, 1H) 8. 49–8.47 (d, J = 6.8 Hz, 2H), 8.16 (s, 1H), 6.85–6.83 (d, J = 7.6 Hz, 2H), 3.17 (s, 6H). ^{13}C NMR (400 MHz DMSO-d_6, ppm): 177.98, 163.19, 155.93, 154.63, 150.77, 139.52, 120.45, 111.67, 110.03. FTIR (ATR, cm^{-1}): 3499.50 (N–H stretching), 3049.93 (C–H stretching), 1684 (C=O stretching). TOF HRMS ES + Calculated for $C_{13}H_{13}N_3O_2S$: 275.3179 Found: 276.0383 $[M + H]^+$.

5-(4-*N,N*-Dimethylaminobenzylidene)-1,3-diethyl-2-thioxo-dihydro-pyrimidine-4,6-dione (A4) Red solid crystallized from ether and ethyl acetate, yield 85%. ^{1}HNMR (400 MHz DMSO-d_6, ppm): 8.48–8.46 (d, J = 8.8 Hz, 2H), 8.27 (s, 1H), 6.88–6.85 (d, J = 8.8 Hz, 2H), 4.46 (s, 4H), 3.19 (s, 6H), 1.22 (s, 6H), ^{13}CNMR (400 MHz DMSO-d_6, ppm): 190.41, 159.30, 158.55, 155.54, 140.49, 112.08, 111.54, 109.27, 43.23, 12.77, FTIR (ATR, cm^{-1}): 3055.08 (C–H stretching), 1682 (C=O stretching).TOF HRMS ES + Calculated for $C_{17}H_{21}N_3O_2S$: 331.4215. Found: 332.1474 $[M + H]^+$.

Results and discussion

Synthesis and structure characterization

The synthetic pathways of the four dyes are depicted in Scheme 1. We have used Knoevenagel condensation protocol to obtain final compounds. The inexpensive starting compound 4-(*N*,*N*-dimethyl amino)benzaldehyde (**S**) was reacted with selected anchoring molecules, viz. barbituric acid, 1,3-dimethylbarbituric acid, thiobarbituric acid and 1,3-diethylthiobarbituric acid to yield target molecules **A1**–**A4** in good yield. The melting point and spectral data of dyes **A1**–**A4** match with reported values [23, 24].

Crystal structure

*Crystal structure of 5-(4-N,N-dimethylamino-benzylidene)-1,3-diethyl-2-thioxo-dihydro-pyrimidine-4,6-dione (**A2**)*

High-quality orange-colored single crystal of **A2** was obtained by slow evaporation of its solution with 1:1 pet ether (60–80 °C)/ethyl acetate solvent mixture. The single crystal was subjected to SC-XRD analysis, and obtained crystal data are presented in Table 1. The SC-XRD studies reveal that dye **A2** crystallizes in triclinic space group *P*-1 with cell parameters, a = 8.7515(3) (Å), b = 8.9890(3) Å, c = 9.0880(3) Å, V = 696.81(4) Å^3, Z = 2. Figure 1a shows the ORTEP diagram of the dye **A2**.

*Crystal structure of 5-(4-N,N-dimethyl-amino-benzylidene)-1,3-diethyl-2-thioxo-dihydro-pyrimidine-4,6-dione (**A4**)*

Superior-quality shining red-colored single crystal of dye **A4** was obtained by very slow evaporation of its solution with 1:1 pet ether (60–80 °C)/ethyl acetate solvent mixture. SC-XRD analysis was carried out, and obtained crystal

Table 1 Crystal and structure refinement data for dyes **A2** and **A4**

Compound	**A2**	**A4**
Formula	$C_{15}H_{17}N_3O_3$	$C_{17}H_{21}N_3O_2S$
Formula weight	287.32	331.43
CCDC number	1,456,338	1,490,875
Temperature (K)	296 (2)	296 (2)
Crystal form	Block	Block
Color	Orange	Red
Crystal system	Triclinic	Triclinic
Space group	*P*-1	*P*-1
a (Å)	8.7515 (3)	7.9072 (2)
c (Å)	9.0880 (3)	10.3716 (3)
a (0)	81.822 (2)	88.3470 (10)
b (0)	81.299 (2)	79.4360 (10)
g (0)	83.835 (2)	86.0360 (10)
Volume (Å^3)	696.81 (4)	823.95 (4)
Z	2	2
Density (g cm^{-3})	1.369	1.336
μ (mm^{-1})	0.097	0.210
F (000)+	304	352
$h_{min, max}$	−10, 10	−9, 9
$k_{min, max}$	−11, 10	−12, 12
$l_{min, max}$	−11, 11	−12, 12
Reflections collected	2736	3239
R_{all}, R_{obs}	0.0541, 0.0441	0.0440, 0.0393
wR2$_{-all}$, wR2$_{-obs}$	0.1350, 0.1207	0.1281, 0.1197
GOOF	0.674	0.835

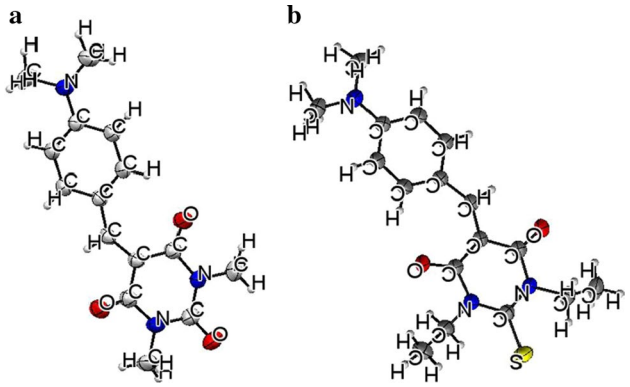

Fig. 1 **a** ORTEP diagram of dye **A2**, **b** ORTEP diagram of dye **A4**

data are presented in Table 1. The SC-XRD studies indicate that dye **A4** crystallizes in triclinic space group *P*-1 with cell parameters, $a = 7.9072(2)$ (Å), $b = 10.2460(3)$ Å, $c = 10.3716(3)$ Å, $V = 823.95(4)$ Å^3, $Z = 2$. Figure 1b depicts the ORTEP diagram of the dye **A4**, from which it is quite evident that the dye is almost planar, which favors the flow of electron density from the donor segment to the acceptor segment through the π-conjugation bridge and thereby enhancing overall efficiency of the sensitizers.

Photophysical properties

The UV–visible absorption and photoluminescence emission spectra of dyes **A1**–**A4** were recorded in chloroform solution at a concentration of 10^{-5} M. Figures 2 and 3 depict the UV–visible absorption and photoluminescence emission spectra of **A1**–**A4**, respectively. The relevant spectral results are presented in Table 2. From the absorption spectra, it is

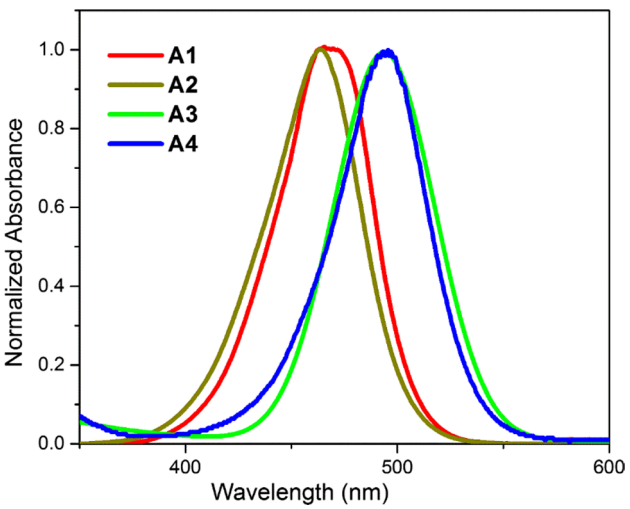

Fig. 2 UV–visible absorption spectra of dyes **A1**–**A4** at 10^{-5} M concentration

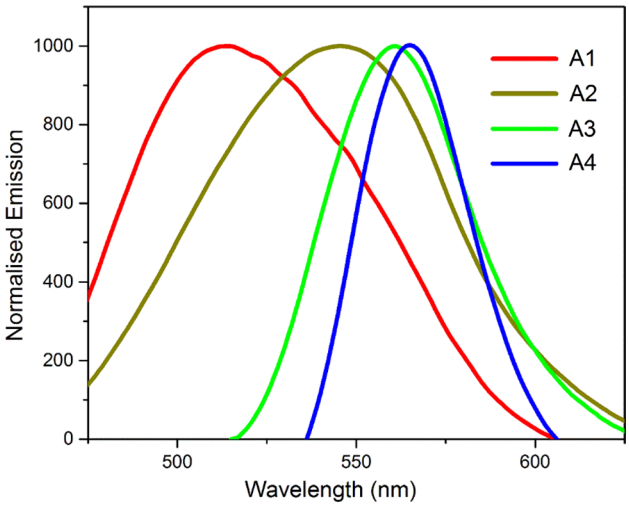

Fig. 3 Fluorescence emission spectra of dyes **A1**–**A4 at** 10^{-5} M concentration

clear that the dyes **A1** and **A2** exhibit single distinct absorption band, while dyes **A3** and **A4** display two major absorption bands. In case of compounds **A1** and **A2**, the single peak at around 470 nm is attributed to the intramolecular charge transfer (ICT) from donor, i.e., 4-(*N,N*-dimethylamino)phenylene group, to the corresponding acceptor unit, i.e., barbituric acid or *N,N*-dimethyl barbituric acid. While the dyes **A3** and **A4** show absorption bands in the shorter wavelength (250 and 350 nm) corresponding to π–π* electronic excitations localized within the 4-(*N,N*-dimethylamino)phenylene group, whereas the intense band in the longer wavelength region (496 and 500 nm) can be attributed to an intermolecular charge-transfer (ICT) transition from the donor to the acceptor segment [25]. The observed values of molar extinction coefficients in all the sensitizers ranging from 32,000 to 83,000 M^{-1} cm^{-1} endorse their fairly good light-harvesting ability. Further, the calculated Stoke shift values for the sensitizers **A1**–**A4** were found to be fairly large, i.e., 41–79 nm, which can be ascribed to the moderate charge transfer from the donor to the acceptor unit.

Electrochemical measurements

Cyclic voltammetry (CV) experiments were carried out in order to determine the ground-state oxidation potential (GSOP) and excited-state oxidation potential (ESOP) values of the synthesized sensitizers (**A1**–**A4**). These values offer a deeper insight into the thermodynamic driving force of electron injection from the ESOP of dye molecule into the conduction band edge of semiconductor TiO_2 and dye regeneration via replenishing the hole generated in the GSOP by the redox electrolyte. The cyclic voltammetric traces of the dyes **A1**–**A4** were recorded using Ivium Vertex electrochemical

Table 2 Optical and electrochemical characterization data of dyes **A1**–**A4**

Dye	λ_{abs} (nm)	λ_{em} (nm)	Stokes shift (nm)	ε (M^{-1} cm^{-1})	E_{ox} (V)	E_{0-0}, optical (eV)	HOMO (eV)	LUMO (eV)
A1	473	514	41	32,000	1.25	2.54	−5.65	−3.11
A2	467	546	79	45,500	0.78	2.57	−5.18	−2.67
A3	500	561	61	59,000	1.12	2.35	−5.52	−3.17
A4	498	566	68	83,000	0.89	2.36	−5.29	−2.93

λ_{abs}, Absorption maxima; λ_{em}, emission maxima; E_{ox}, oxidation potential; E_{0-0}, voltage of intersection point between absorption and emission spectra

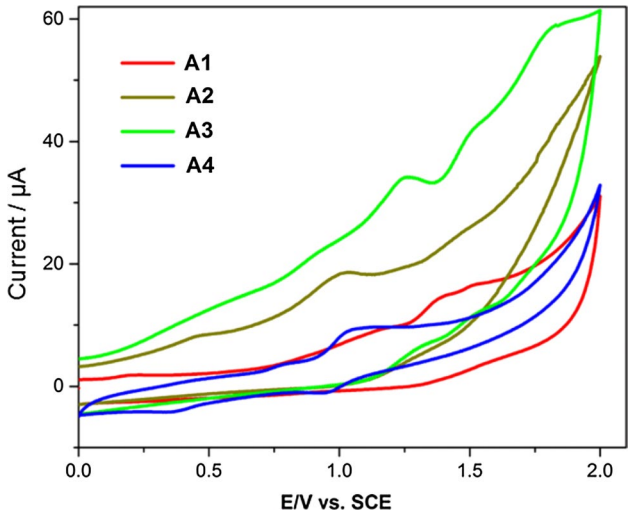

Fig. 4 CV traces of dyes **A1**–**A4**

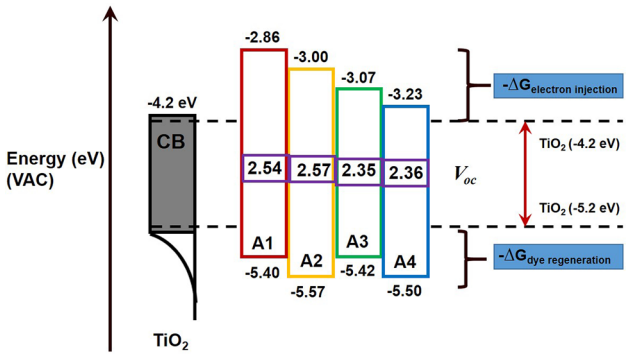

Fig. 5 Energy-level diagram of dyes **A1**–**A4**

workstation. A thin film of the dye was obtained from the dye solution using drop-cast method on a glassy carbon electrode, which works as working electrode. Experiments were performed using Pt electrode as a counter electrode and Ag/AgCl as a reference electrode, immersed in an electrolyte [0.1 M tetrabutylammonium tetrafluoroborate in acetonitrile] at a scan rate of 100 mV/s. The obtained cyclic voltammograms of **A1**–**A4** are displayed in Fig. 6, and the corresponding values are summarized in Table 2 (Fig. 4).

The obtained CV data were used to compute the oxidation onset values (GSOP). The energy gap of the dye, E_{0-0}, was calculated from its absorption and normalized emission spectra. Further, E_{0-0} and GSOP values were employed to calculate the excited-state oxidation potential (ESOP); the values in volts (V) against NHE were converted to electron volt (eV) according to the following equation [26–28]:

$$\text{ESOP} = \left[(\text{GSOP(V)} + 4.7) - E_{0-0}\right] \text{eV}$$

Figure 5 depicts the energy-level diagram, showing the GSOP and ESOP values of **A1**–**A4** dyes. It has been observed that GSOP values of dyes **A1** (−5.40 eV), **A2** (−5.57 eV), **A3** (−5.42 eV) and **A4** (−5.59 eV) are lower than those of I_3^-/I^- redox system (−5.2 eV) [29], thus providing ample driving force for effective dye regeneration. In addition, ESOP of **A1** (−2.86 eV), **A2** (−3.00 eV), **A3** (−3.07 eV) and **A4** (−3.23 eV) was found to be higher in energy than the conduction band edge of mesoporous TiO_2 (−4.2 eV) [30], showing an efficient electron injection. Evidently, electron injection free energy for dyes is in the order, i.e., **A4** > **A2** > **A3** > **A1**, while dye regeneration free energy for them is in the same order, due to the fact that all the dyes have similar electron-donating group as well as almost alike HOMO delocalization [31].

As per earlier reports, under optimized conditions, electron injection free energy greater than 150 meV should result in efficient electron injection [32] and dye regeneration free energy as low as 250 meV must lead to efficient dye regeneration. All the synthesized dyes meet stringent thermodynamic requirements, as shown in energy-level diagram (Fig. 5). Further, it has been observed that negative free energy for electron injection is the highest for **A1**. Also, its dye regeneration free energy was found to be the lowest. Accordingly, **A1** showed the highest efficiency among the four dyes. In case of the dye **A3**, the negative free energy for injection is almost same as that of **A1**, predicting that the latter will be almost same efficient as the former. This is also attributed to the observed lowest band gap for **A3,** whereas the other two dyes **A2** and **A4** showed lower efficiency as predicted from their observed free energy values.

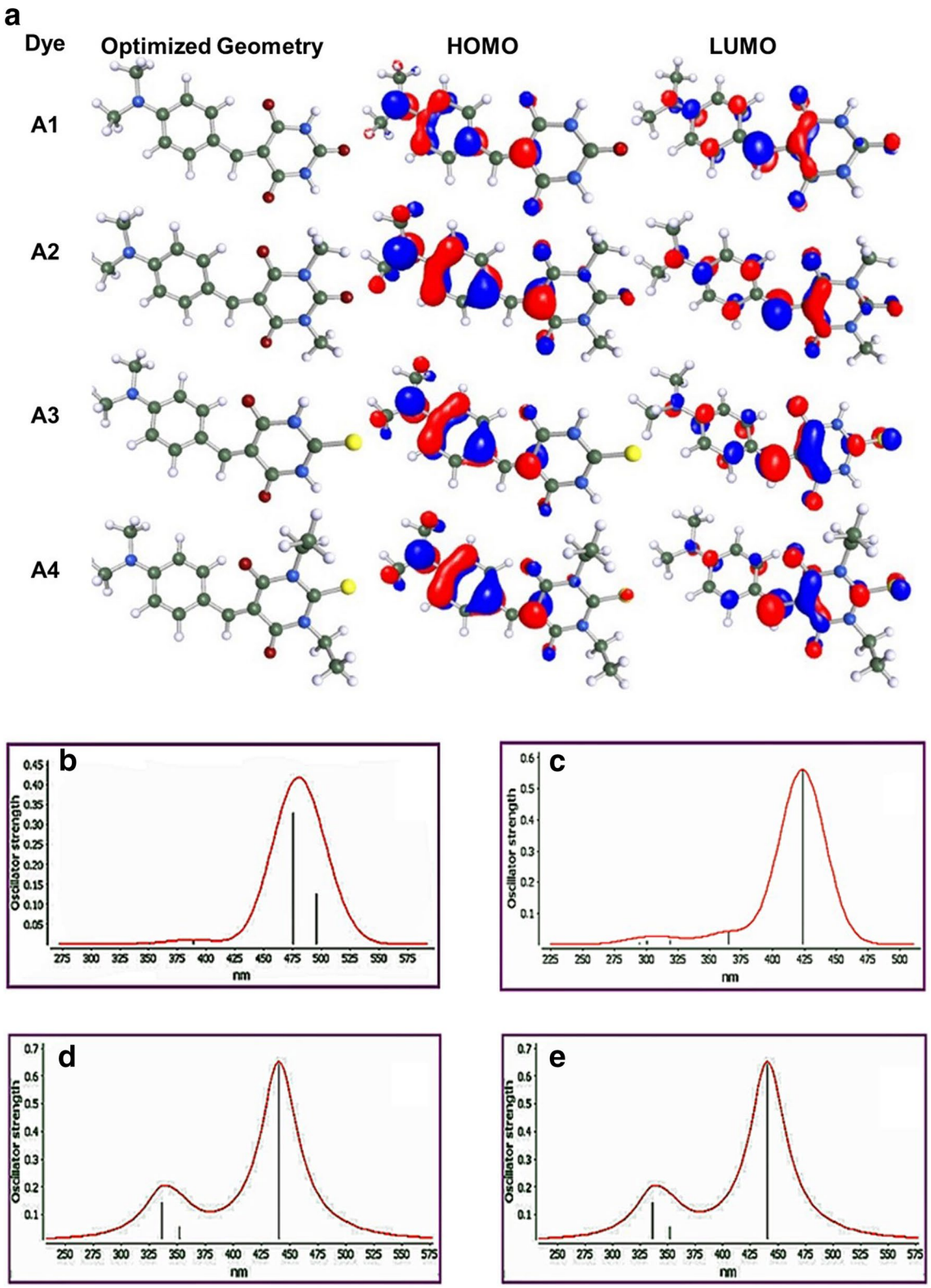

Fig. 6 **a** Optimized structures and frontier molecular orbitals (HOMO and LUMO) of dyes **A1**–**A4**, **b**–**e** simulated absorption spectra of dyes **A1**–**A4**, **f**–**i** simulated vibration spectra of dyes **A1**–**A4**

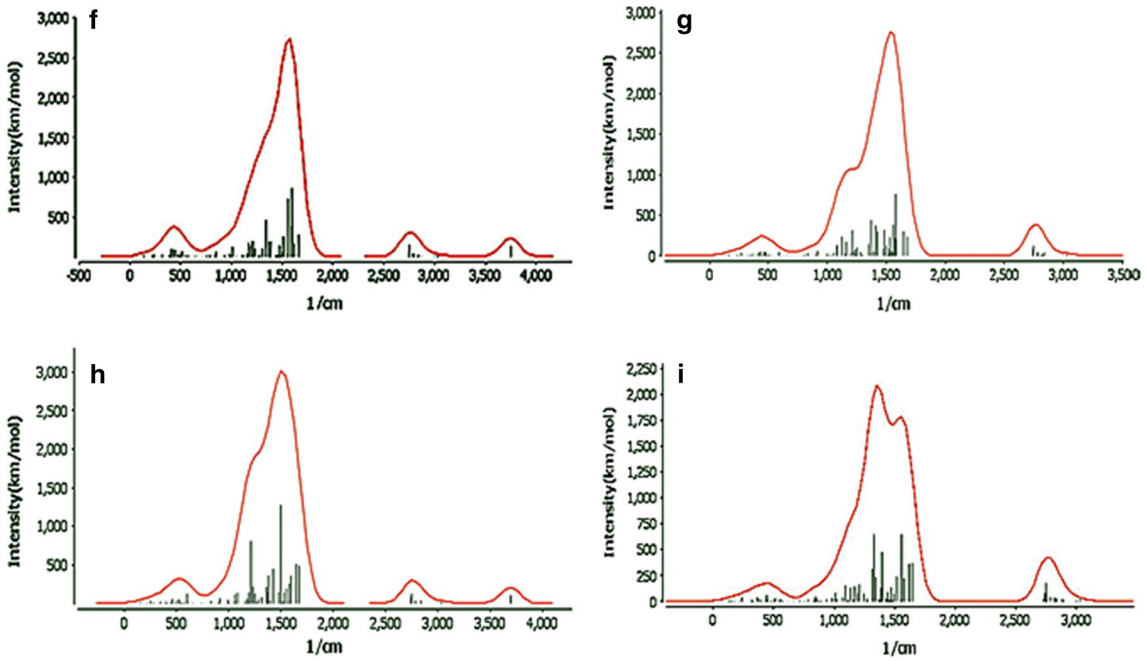

Fig. 6 (continued)

Theoretical calculation

DFT and TD-DFT calculations were performed for all the dyes using Turbomole V7.1 software in order to gain deeper understanding of the electronic and optical properties of the molecules. To begin with, the ground-state geometries were optimized with semiempirical AM1 basis with MOPAC in TmoleX. Further optimization of the aforementioned geometries was performed using C1 point group symmetry at DFT level via the Becke's three-parameter hybrid functional and Lee–Yang–Parr's gradient-corrected correlation functional (B3LYP) [33, 34]. Furthermore, in all the calculations, default convergence criteria were maintained for the optimizations. All calculations were performed using def-TZVPP basis set. The optimized geometries and electron density distributions in the HOMOs and LUMOs of the four dyes are summarized in Fig. 6a. As evidenced from Fig. 6a, in the HOMO level, the electron density is mainly located on the 4-*N,N*-dimethylaniline segment of all the molecules, whereas in the corresponding LUMOs, a clear shift of electron density toward acceptor group, i.e., barbituric acid, *N,N*-dimethyl barbituric acid, thiobarbituric acid and *N,N*-diethyl thiobarbituric acid, is observed. Thus, a close proximity of the LUMO levels to the anchoring group would facilitate considerable orbital overlap between the LUMO levels and 3*d* orbitals of titanium. This would ease efficient injection of excited electrons into conduction band of TiO_2.

Further, time-dependent density functional theory (TD-DFT) studies were conducted to examine the electronic excitations of dyes in the presence of time-dependent perturbations. Typically, in TD-DFT, a time-dependent Schrödinger equation is solved to obtain the excited-state properties of the material. Here, an adiabatic approximation is made and following which temporal non-locality is neglected. According to the aforementioned approximation, at any point of time, the exchange–correlation (xc) functional depends only on the instantaneous density [35].

As a result of aforementioned approximation, traditional approximations (time independent) can be applied to the xc-functional derived for ground-state DFT, i.e., BP (Becke–Perdew) and hybrid functionals (B3LYP) [34]. Typically, the precision of the results acquired using TD-DFT profoundly depends on the functional and basis set employed for the calculations. The simulated absorption spectrum of **A1** obtained at the B3LYP functional and def-TZVPP basis set is depicted in Fig. 6b. Indeed, TD-DFT is known for its inabilities in precisely predicting energies related to long-range charge-transfer states due to the self-interaction error in TD-DFT, which is owing to the electron transfer in the extended charge-transfer state. The above-mentioned variance is not observed in the present study, as the molecules under investigation are not large enough to display a long-range intramolecular charge transfer. Figure 6b portrays the simulated absorption spectrum of **A1** obtained at the B3LYP functional. It shows only one peak, corresponding to its charge-transfer process. Similarly, **A2** displays only one peak as given in Fig. 6c. Simulated absorption spectra of **A3** and **A4** are given in Fig. 6d, e, respectively, from

which it is evident that the molecules exhibit two distinct bands, corresponding to π–π^* and charge-transfer phenomenon. The simulated data are well in accordance with the experimentally obtained spectra. These precise and reliable predictions made by TD-DFT studies indicate that the functional and basis set chosen for TD-DFT calculations are quite appropriate.

Further, the stimulated vibration spectrum was obtained using the B3LYP functional at the def-TZVPP basis set. Figure 6f, h depicts the simulated vibration spectra of **A1** and **A3** obtained at the B3LYP functional. As observed from the simulated spectra of **A1** and **A3**, the molecules exhibit a broad peak at around 3600 cm^{-1} that correspond to NH functionality of the dyes. The obtained data match with the experimental spectral data. Further, the simulated vibration spectra of **A2** and **A4**, as depicted in Fig. 6g, i, respectively, clearly show the absence of NH functionality in the dyes. Henceforth, the theoretically obtained UV–visible and vibration spectral data are in good agreement with the experimentally acquired spectra.

Photovoltaic characterization

In order to establish the structure–performance relationship for synthesized dyes (**A1**–**A4**), DSSCs were fabricated as per the protocol [36, 37] described in supplementary information. In the experiment, dye solutions were prepared in a particular concentration and directly used for device fabrication studies. The current–voltage (*J*–*V*) plots were obtained by using Keithley 2400 source meter under illumination of AM 1.5G solar light from a solar simulator (SOL3A, Oriel). Figure 7 shows *J*–*V* curves of sensitizers **A1**–**A4**-based DSSCs under AM 1.5G simulated sunlight with a light intensity of 100 mW/cm^2. The observed photovoltaic parameters, viz. open-circuit photovoltage (V_{OC}), short-circuit photocurrent density (J_{SC}), fill factor (FF) and overall solar light to electricity conversion efficiency (η), are summarized in Table 3. From the results, it is clear that all the dyes show low J_{SC} and

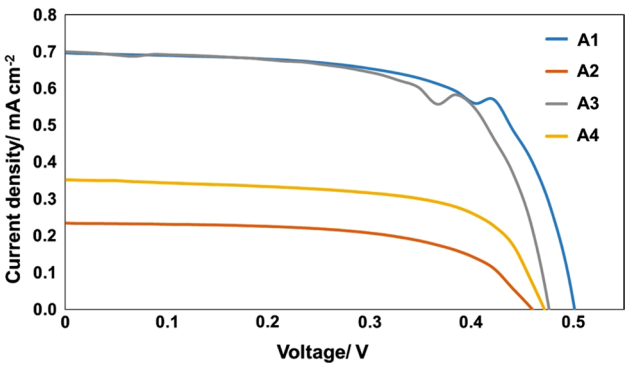

Fig. 7 *J*–*V* characteristics of the DSSCs sensitized with dyes **A1**–**A4**

Table 3 Photovoltaic measurement data of dyes **A1**–**A4**

Dye	V_{OC} (V)	J_{SC} (mA cm^{-2})	FF %	η %
A1	0.501	0.70	67.0	0.244
A2	0.460	0.23	60.4	0.065
A3	0.476	0.70	67.1	0.223
A4	0.472	0.35	64.5	0.108

V_{OC} values mainly due to their heavy aggregation on the surface of TiO_2. Among the tested dyes, the dye **A1** displayed maximum efficiency of 0.244% due to the strong binding of barbituric acid on TiO_2. While the dye **A2** showed the lowest efficiency of 0.065% due to the non-availability of free NH group to bind on the surface of mesoporous TiO_2 effectively. The dye **A3** exhibited an efficiency 0.223% comparable to that of **A1**, owing to binding of sulfinyl as well as NH group, whereas the dye **A4** disclosed an efficiency of 0.108%, which is attributed to non-availability of free NH functionality. Compared to **A1** and **A3**, the binding strength of **A2** and **A4** on TiO_2 surface is weak. The possible binding mode for **A2** and **A4** is monodentate coordinating mode through a C=O or C=S group with Ti on the TiO_2 surface, while in **A1** and **A3**, the binding mode is bidentate bridging due to the tautomeric forms [38]. The weak binding strength caused insufficient electron injection from the sensitizer to the TiO_2, leading to the decrease of Jsc and the overall efficiency. The results obviously indicate that conversion efficiency of all the dyes is not promising, even though they display good photophysical and electrochemical properties. It has been well established that one of the striking phenomena, i.e., dye aggregation, significantly influences its electron injection behavior [39], causing adverse effect on the overall performance of DSSCs. Evidently, the absence of long-chain bulky groups in the dyes **A1**–**A4** has favored the excessive aggregation allowing the electrolyte to interact directly with the TiO_2 and hence instigating back current in the cell [18, 40]. In conclusion, the absence of long hydrophobic chains results in the facilitated dye aggregation and undesired charge recombination, leading to the decrease of V_{OC} values and the overall efficiencies.

Conclusions

We have synthesized four structurally simple organic D–A-type sensitizers (**A1**–**A4**), based on the donor *N*,*N*-dimethyl-4-vinyl aniline carrying four different acceptor/anchoring groups, viz. barbituric acid, *N*,*N*-dimethyl barbituric acid, thiobarbituric acid and *N*,*N*-diethyl thiobarbituric acid, for DSSC application. The synthesized dyes were subjected to photophysical, electrochemical, theoretical and device fabrication studies. The results reveal that the dyes show

good absorption/emission property and enhanced thermodynamic feasibility of their electron injection into the conduction band of TiO_2 followed by dye regeneration. Their electronic distribution in HOMO and LUMO levels indicates that, in the HOMO, the electron density is delocalized over the entire molecule, while in the LUMO a clear shift of electron density toward the acceptor segment is observed. Such movement of electron density is quite suitable and desirable for efficient charge transfer. Relatively good efficiency of DSSCs sensitized with **A1** and **A3** when compared to other two dyes is due to the effective binding of barbituric and thiobarbituric acid on the surface of TiO_2 through NH or OH functional groups. Their lower J_{SC} and V_{OC} values can be accounted for heavy aggregation of dye molecules on the surface of TiO_2 mainly due to the absence of bulky side chains in the molecules.

Supplementary information

All structural characterization, DFT calculations and crystal data are available in electronic supplementary data.

Acknowledgements The authors are thankful to National Institute of Technology, Surathkal, India, for providing necessary laboratory facilities. The authors are also thankful to the Department of Textile Engineering, Chemistry and Science at North Carolina State University for the financial support.

References

1. B. O'Regan, M. Grätzel, Nature **353**, 737 (1991)
2. Y. Ooyama, Y. Harima, Eur. J. Org. Chem. **2009**, 2903 (2009)
3. S. Mathew, A. Yella, P. Gao, R. Humphry-Baker, B.F.E. Curchod, N. Ashari-Astani, I. Tavernelli, U. Rothlisberger, M.K. Nazeeruddin, M. Grätzel, Nat. Chem. **6**, 242 (2014)
4. A. Mishra, M.K.R. Fischer, P. Bäuerle, Angew. Chem. Int. Ed. **48**, 2474 (2009)
5. J.N. Clifford, E. Martínez-Ferrero, A. Viterisi, E. Palomares, Chem. Soc. Rev. **40**, 1635 (2011)
6. D.P. Hagberg, T. Marinado, K.M. Karlsson, K. Nonomura, P. Qin, G. Boschloo, T. Brinck, A. Hagfeldt, L. Sun, J. Org. Chem. **72**, 9550 (2007)
7. M. Liang, W. Xu, F. Cai, P. Chen, B. Peng, J. Chen, Z. Li, J. Phys. Chem. C **111**, 4465 (2007)
8. W. Xu, B. Peng, J. Chen, M. Liang, F. Cai, J. Phys. Chem. C **112**, 874 (2008)
9. C.-H. Yang, H.-L. Chen, C.-P. Chen, S.-H. Liao, H.-A. Hsiao, Y.-Y. Chuang, H.-S. Hsu, T.-L. Wang, Y.-T. Shieh, L.-Y. Lin, Y.-C. Tsai, J. Electroanal. Chem. **631**, 43 (2009)
10. G. Reginato, M. Calamante, A. Dessì, A. Mordini, M. Peruzzini, L. Zani, J. Organomet. Chem. **771**, 117 (2014)
11. S. Urnikaite, M. Daskeviciene, R. Send, H. Wonneberger, A. Sackus, I. Bruder, V. Getautis, Dyes Pigm. **114**, 175 (2015)
12. T. Michinobu, N. Satoh, J. Cai, Y. Li, L. Han, J. Mater. Chem. C **2**, 3367 (2014)
13. M. Komatsu, J. Nakazaki, S. Uchida, T. Kubo, H. Segawa, Phys. Chem. Chem. Phys. **15**, 3227 (2013)
14. M. Subbaiah, R. Sekar, E. Palani, A. Sambandam, Tetrahedron Lett. **54**, 3132 (2013)
15. S. Manoharan, S. Anandan, Dyes Pigm. **105**, 223 (2014)
16. V.P. Novikov, S. Samdal, L.V. Vilkov, Russ. J. Gen. Chem. **74**, 1247 (2004)
17. D.D. Babu, R. Su, A. El-Shafei, A.V. Adhikari, Electrochim. Acta **10**, 198 (2016)
18. B. Hosseinzadeh, A. Salimi Beni, A. Najafi Chermahini, R. Ghahary, A. Teimouri, Synth. Met. **209**, 1 (2015)
19. S. Wang, S.-H. Kim, Dyes Pigm. **80**, 314 (2009)
20. Y. Hu, Z.-C. Chen, Z.-G. Le, Q.-G. Zheng, Synth. Commun. **34**, 4521 (2004)
21. M.K. Haldar, M.D. Scott, N. Sule, D.K. Srivastava, S. Mallik, Bioorg. Med. Chem. Lett. **18**, 2373 (2008)
22. Z. Wu, W. Ma, S. Meng, X. Li, J. Li, Q. Zou, J. Hua, H. Tian, RSC Adv. **6**, 74039 (2016)
23. M.C. Rezende, P. Campodonico, E. Abuin, J. Kossanyi, Spectrochim. Acta Part A Mol. Biomol. Spectrosc. **57**, 1183 (2001)
24. C. Saravanan, S. Easwaramoorthi, L. Wang, Dalton Trans. **43**, 5151 (2014)
25. D.D. Babu, R. Su, P. Naik, A. El-Shafei, A.V. Adhikari, Dyes Pigm. **141**, 112 (2017)
26. P. Naik, R. Su, M.R. Elmorsy, D.D. Babu, A. El-Shafei, A.V. Adhikari, J. Photochem. Photobiol. A **345**, 63 (2017)
27. P. Naik, M.R. Elmorsy, R. Su, D.D. Babu, A. El-Shafei, A.V. Adhikari, Sol. Energy **153**, 600 (2017)
28. D.D. Babu, D. Elsherbiny, H. Cheema, A. El-Shafei, A.V. Adhikari, Dyes Pigm. **132**, 316 (2016)
29. P. Qu, G.J. Meyer, Langmuir **17**, 6720 (2001)
30. G. Oskam, B.V. Bergeron, G.J. Meyer, P.C. Searson, J. Phys. Chem. B **105**, 6867 (2001)
31. V. Gaidelis, E. Kamarauskas, T. Malinauskas, V. Getautis, R. Send, H. Wonneberger, I. Bruder, RSC Adv. **5**, 82859 (2015)
32. S.E. Koops, B.C. O'Regan, P.R.F. Barnes, J.R. Durrant, J. Am. Chem. Soc. **131**, 4808 (2009)
33. A.D. Becke, Phys. Rev. A **38**, 3098 (1988)
34. M.J.G. Peach, P. Benfield, T. Helgaker, D.J. Tozer, J. Chem. Phys. **128**, 04418 (2008)
35. P. Dev, S. Agrawal, N.J. English, J. Phys. Chem. A **117**, 2114 (2013)
36. D. El-Sherbiny, H. Cheema, F. El-Essawy, A. Abdel-Megied, A. El-Shafei, Dyes Pigm. **115**, 81 (2015)
37. P.M. Sirimanne, H. Tributsch, J. Solid State Chem. **177**, 1789 (2004)
38. L. Zhang, J.M. Cole, A.C.S. Appl, Mater. Interfaces **7**, 3427 (2015)
39. K.R. Justin Thomas, A. Venkateswararao, C.-P. Lee, K.-C. Ho, Dyes Pigm. **123**, 154 (2015)
40. K. Zhou, H. Fu, L. Feng, M. Cui, J. Dai, B. Liu, Chem. Commun. **51**, 11665 (2015)